SMGroup

Recent Advances in Neural Connectivity Inference Problem for Very Large Scale Population Calcium Imaging

Yuriy Mishchenko[1]*

[1]Izmir University of Economics, Faculty of Engineering, Turkey

***Corresponding author:** Yuriy Mishchenko, Izmir University of Economics, Faculty of Engineering, Sakarya Cd. 156, 35330 Balcova- Izmir, Turkey, Email: yuriy.mishchenko@gmail.com

Published Date: September 25, 2016

ABSTRACT

Recent years had seen important advances in the computational problem of deconvolution of calcium imaging signals as well as estimation of neural connectivity from population calcium imaging data. In experimental domain, calcium imaging had scaled up tremendously, with imaging of neural populations on the scale of entire brain in alive and behaving animals recently demonstrated. Solutions for neural connectivity inference from very large-scale calcium imaging data had been also offered. A particularly important advance can be seen in the recent introduction in computational neuroscience literature of the concept of sparse neural population imaging and connectivity inference. These advances make it now possible to pursue calcium imaging-based reconstructions of neural connectivity in macroscopically large neural circuits or even the entire brain. This chapter provides a technical overview of some of the important recent

advances in computational connectivity inference from very large-scale population calcium imaging data, emphasizing specifically the opportunities that became open in population calcium imaging thanks to such advances. I discuss the current status of the problem of computational deconvolution of calcium imaging signals, inference of neural connectivity from population calcium imaging data, and recent advances related to sparse or "shotgun" neural activity imaging. I introduce a theoretical framework, based on the notion of effective connectivity models of neural population activity, which can be used to fruitfully combine these computational advances with experimental large-scale population calcium imaging developments. Together with this framework, the concepts and techniques described in this chapter can serve as the foundation for rapid advancements in quantitative understanding of the workings of neural circuits in the brain.

INTRODUCTION

One of the key challenges of neuroscience is to understand how the structure of neural circuits forms the substrate for information processing in the brain. Since the times of Ramon y Cajal [1,2], neuroscientists have been curious about how the neural networks in the brain work and how they provide the biological foundation of memory, cognition, and perception. While we have learned a lot about these questions in the last century, a number of questions remain about the nature of the "micro-circuits" in the brain, i.e., the connectivity within the populations of neurons at single-cell level. It is universally accepted in neuroscience that neurons and their electrochemical connections constitute the fundamental blocks of the neural processing in the brain. Thus, uncovering the information about the connectivity and the dynamics of individual neurons in the brain arguably constitutes the fundamental way for reproducing the high-level behaviors observed in the brain, as is embodied, for instance, by the Blue Brain project [3].

It comes of no surprise, thus, that a significant effort became directed at directly imaging neural connectivity in past years [4-12], funneling recently into two large brain imaging initiatives in the US [13] and Europe [14]. Two complementary approaches have been pursued in neuroimaging for that purpose. A number of anatomical studies had focused on extracting the neuronal connectivity graph directly by identifying how neurons are physically connected [6,8,12,15-18]. Functional studies, on the other hand, rely on the analysis of neural activity observed via techniques such as multi-electrode local field potential recordings [19-26], voltage imaging [27-29] or calcium imaging [30-52]. Although functional approaches have not been demonstrated to directly yield the physical structure of neural circuits, this type of analysis plays an increasingly important role in our attempts to understand the information processing in the neural circuits by offering information about the dynamical properties of neurons and their interactions, which is absent from purely anatomical approaches [5,7,26,53-58].

Experimental tools allowing simultaneous observation of activity of many neurons has underwent dramatic developments in recent years. Arrays of extracellular electrodes had been scaled to very large sizes [26,53,58], while calcium fluorescence-based neural population activity

imaging had scored incredible fits including whole brain imaging in some biological systems [36,40,42-44,46,48-51]. Very large-scale calcium fluorescence imaging can be now performed using either organic or genetic calcium-sensitive fluorescent indicators [30-33,59,60], observed at high frame rates using wide-field CCDs [61] or laser scanning microscopy [62-66]. Together, these tools had provided movies of calcium fluorescence from networks of neurons as large as the entire central nervous system in the systems including *C. elegans* [36,40], larval Drosophila [42,48], and larval zebrafish [36,43,46,49,50]. These experimental advances now allow studying the organization of neuronal circuits at single-cell level using powerful advanced statistical techniques [54,67-77].

This chapter provides a technical overview of some of the recent results produced in functional connectivity inference problem for very large-scale population calcium imaging, emphasizing specifically the opportunities that became open in recent years in population calcium imaging thanks to several such advances. I discuss the current status of the computational problem of neural connectivity inference using calcium imaging data as well as certain recent progress related to neural connectivity inference from calcium imaging data of very large scale, such as the whole-brain calcium imaging data, by means of using sparse or "shotgun" neural activity imaging approaches [78,79]. I introduce the theoretical framework of effective connectivity modeling for such inference, which can provide the theoretical basis for use of such approaches in neuroscience and contribute to quantitative and principled realization of the "*Observe-Explain-Predict*" scientific method cycle in neuroscience to understand the workings of neural circuits at single-neuron level.

CONNECTIVITY RECONSTRUCTIONS FROM POPULATION CALCIUM IMAGING

Theoretical and Computational Background

The problem of neural connectivity analysis from functional data such as the neuronal spike trains identified from local field potential recordings or calcium imaging has long standing in computational neuroscience. In the case of the calcium imaging data, this problem consists of two parts: the deconvolution of slow and often noisy calcium fluorescence signal into underlying neuronal spike trains and the estimation of the connectivity graph from thus obtained spike trains.

The computational foundation for solving this problem is provided by the mathematical model of calcium fluorescence signal and the neural population activity, which in the most general form can be described by the set of equations below,

$$
\begin{aligned}
&S_i(t) \sim P\left(S_i(t) \middle| H_i^{(s)}(t), H^{(n)}(t); \zeta_i, W_i\right), \\
&n_i(t) \sim P\left(n_i(t) \middle| S_i(t), \zeta_i\right), \\
&C_i(t) \sim P\left(C_i(t) \middle| n_i(t), H_i^{(c)}(t); \vartheta_i\right), \\
&F_i(t) \sim P\left(F_i(t) \middle| C_i(t); \vartheta_i\right), i = 1, ..., N.
\end{aligned} \tag{1}
$$

In Eq. (1), the first two equations define the statistical model of spiking neural activity in a population of N neurons i=1,...,N. The first equation is the dynamical model of individual neurons' states, $S_i(t)$, which describes the evolution of the quantities controlling the spiking of neurons such as various ionic currents in conductance-based neural activity models or membrane voltage in a Leaky Integrate and Fire **(LIF)** models. The state evolution naturally depends on the past internal states of the same neuron $H_i^{(s)}(t)$ as well as the past spikes of the entire neural population $H^{(n)}(t)$, whereas the spikes thus form the only externally "exposed" state variables in this neural population dynamics model. The second equation for $n_i(t) \in \{0,1\}$ describes the spiking process in neurons. This equation encodes the details of neural spiking in relation to internal states $S_i(t)$. The parameters ζ and W are the dynamic parameters; W typically is associated with the interactions between neurons and is described as a connectivity matrix or a graph and ζ describes the dynamical properties of individual neurons.

The second pair of equations in Eq. (1) is the model of calcium dynamics and the fluorescence of calcium indicators. The first equation in that pair describes the evolution of calcium concentrations $C_i(t)$ inside neurons, which depends on past calcium concentrations $H_i^{(c)}(t)$ and the instantaneous spiking state of a neuron $n_i(t)$. The last equation for $F_i(t)$ is the model of calcium indicator's fluorescence. The parameters ϑ characterize the intracellular dynamics of calcium concentrations as well as the fluorescence properties of calcium indicators, for instance, including such parameters as the decay time of calcium transients, the magnitude of spike-triggered jumps in calcium concentrations, etc.

We say that the model of neural population activity (1) is statistical, in the sense that it does not prescribe neural evolution deterministically but rather in terms of probability distributions such as $P\left(S_i(t) \middle| H_i^{(s)}(t), H^{(n)}(t); \zeta_i, W_i\right)$ or $P\left(n_i(t) \middle| S_i(t), \zeta_i\right)$, and causal, in the sense that such distributions depend exclusively on the past events such as encoded by the "history" variables $H^{(n)}(t) = \{n_i(t'), i = 1, ..., N \,\&\, t' < t\}$, $H_i^{(s)}(t) = \{S_i(t'), t' < t\}$, and $H_i^{(c)}(t) = \{C_i(t'), t' < t\}$.

The problem of extracting the neural connectivity graph from population calcium imaging data, therefore, can be generally expressed as the estimation of the connectivity matrix parameter W given a collection of calcium fluorescence imaging data $F = \{F_i(t), i = 1, ..., N \,\&\, t = 1, ..., T\}$ and a model of type (1). The solution to this problem had been approached in the literature in different ways. One very common such an approach is to note that the calcium fluorescence and the neural activity models separate in Eq. (1), in the sense that the calcium transients and fluorescence depend solely on the instantaneous values of the spike variables $n_i(t)$. It may be tempting, therefore, to attack this problem in a modular manner, by first performing the deconvolution of calcium fluorescence signals F into underlying spike-trains $n_i(t)$ while ignoring the dynamics of $n_i(t)$.

A large number of such calcium fluorescence deconvolution algorithms had been proposed in the literature [37,41,66,80-87], also see [66] for a recent survey and a benchmark. Such algorithms typically depart from a linear model of calcium fluorescence,

$$F_i(t) = \alpha_i C_i(t) + \beta_i + \sigma_i^F \varepsilon_i^F(t), \tag{2}$$

where $\varepsilon_i^F(t)$ is a zero-mean and unit-variance Normal random noise variable, and a slow decay-autoregressive model for $C_i(t)$ with the calcium transients' decay time τ_i^c, time-discretization step Δ, and a constant background calcium concentration C_i^b,

$$C_i(t) = C_i(t-\Delta) + \left(C_i^b - C_i(t-\Delta)\right)\Delta / \tau_i^c + n_i(t). \tag{3}$$

In this form, the solution to the deconvolution problem can be straightforwardly produced as a linear filter also known as the Wiener filter. Such solution is computationally and conceptually simple to formulate and evaluate, having a linear time complexity of calculations. The drawback of such a solution is that it is strongly affected by noise in calcium fluorescence data, because the corresponding Wiener deconvolution filter is highly singular. More sophisticated approaches had taken into account various additional information about the dynamics of calcium fluorescence signal, thus reducing the damage produced by noise. In popular Fast Non-Negative Deconvolution Algorithm [82], for example, one supplements Eq. (2) and Eq. (3) with additional condition of non-negativity of $n_i(t)$. This transforms the deconvolution problem into a Linear Program that, although more complex than the Wiener filter above, still can be solved efficiently using standard convex optimization algorithms. A more advanced work [88] makes use of a realistic model of saturating calcium fluorescence and a filter-smoother type Bayesian inference algorithm for estimating the probabilities of binary spikes from calcium fluorescence signals in a Hidden Markov Model setting.

Assuming that the complete raster of the spike trains of a neural population, $\chi = \{n_i(t), i = 1, ..., N \,\&\, t = 1, ..., T\}$, had been obtained from calcium imaging data in the above way, the problem of estimating the connectivity matrix W for the neural population can now be approached by fitting a model of neural activity such as given by Eqs. (1.1)-(1.2) to that

spiking data. One should note that estimating the connectivity matrix W requires necessarily a solution for the dynamical parameters ζ as well - it is not possible to speak about a certain neural connectivity matrix if neural dynamics parameters had not been fixed. Such model fits can be produced by using the Maximum Likelihood Estimation **(MLE)**, in which case the set of model parameters (ζ, W) is determined in a process that maximizes the likelihood of observing the given raster of neural activity,

$$\left(\zeta, W\right) = \arg\max \log P\left(\chi \middle| \zeta, W\right), \tag{4}$$

where $P\left(\chi \middle| \zeta, W\right)$ is generated by means of applying Eqs. (1.1)-(1.2). One popular choice in that setting is the use of Generalized Linear Models **(GLM)** for describing spiking neural activity [67,70,73,75-77,89],

$$n_i\left(t\right) \sim Poisson\left[f\left(b_i + k_i^T . X\left(t\right) + \sum_{j=1}^{N} \sum_{\tau=\Delta}^{\tau_{\max}} W_{ij}\left(\tau\right) n_j\left(t-\tau\right) \right) \right]. \tag{5}$$

This model can be fitted to neural activity data efficiently and for the data of very large size, especially for log-concave rate-functions f (.) [90].

A more principled approach to solving problem (1) involves solving simultaneously the neural dynamics problem (1.1)-(1.2) and the calcium fluorescence problem (1.3)-(1.4). A solution of this type had been offered in [54]. In [54], a Monte-Carlo Expectation-Optimization algorithm had been presented for rigorous Bayesian estimation of neural activity parameters ζ and W as well as the calcium fluorescence parameters ϑ from calcium imaging data. [54] used a realistic GLM of neural activity with autoregressive synaptic currents J_{ij} and a realistic calcium fluorescence model with exponentially decaying calcium transients, saturating calcium indicator's fluorescence, and a realistic optical photon shot-noise model;

$$\begin{aligned}
&J_{ij}\left(t\right) = \left(1 - \Delta / \tau_i^h\right) J_{ij}\left(t-\Delta\right) + \sigma_{ij}^h \sqrt{\Delta} \varepsilon_{ij}^h\left(t\right), \\
&n_i\left(t\right) \sim Bernoulli\left[f\left(b_i + k_i^T . X\left(t\right) + \sum\nolimits_{j=1}^{N} W_{ij} J_{ij}\left(t\right) \right) \right], \\
&C_i(t) = C_i\left(t-\Delta\right) + \left(C_i^b - C_i\left(t-\Delta\right)\right) \Delta / \tau_i^c + A_i n_i\left(t\right) + \sigma_i^c \sqrt{\Delta} \varepsilon_i^c\left(t\right), \\
&F_i\left(t\right) = \alpha_i S\left(C_i\left(t\right)\right) + \beta_i + \sqrt{\left(\sigma_i^F\right)^2 + \gamma_i S\left(C_i\left(t\right)\right)} \varepsilon_i^F\left(t\right),
\end{aligned} \tag{6}$$

where the rate function $f\left(J\right) = 1 - \exp\left(-e^J \Delta\right)$ and the saturating fluorescence function $S\left(C\right) = C / \left(C + K_d\right)$.

A successful application of that algorithm had been demonstrated *in situ* on the simulations of calcium imaging observations of realistic cortical neural micro-circuits with up to 1000 neurons.

Implications For Population Clacium Imaging Experiments

If neural connectivity reconstructions from population calcium imaging data are to be attempted in real biological models, it is important to understand which imaging regimes are required for such reconstructions to be successful. [54] performs a survey of the neural connectivity inference's performance in respect to the key parameters of calcium imaging such as imaging frame rate, signal-to-noise ratio, and imaging duration. Given the rigorous Bayesian nature of the solution algorithm used in that work, that survey can be also viewed as such establishing the performance limits for any neural connectivity inference algorithm in regards to the parameters of a calcium imaging experiment. A similar and somewhat broader study had been performed in [91], with similar conclusions.

Accordingly, it had been found in those studies that the frame rate of calcium imaging places the most stringent constraint on one's ability to extract neural connectivity from calcium imaging data. As is indicated in Figure 1, the frame rate of calcium imaging strongly affects the possibility of connectivity reconstructions, and the frame rates of at least 30 Hz are necessary to extract the connectivity matrix with any meaningful accuracy.

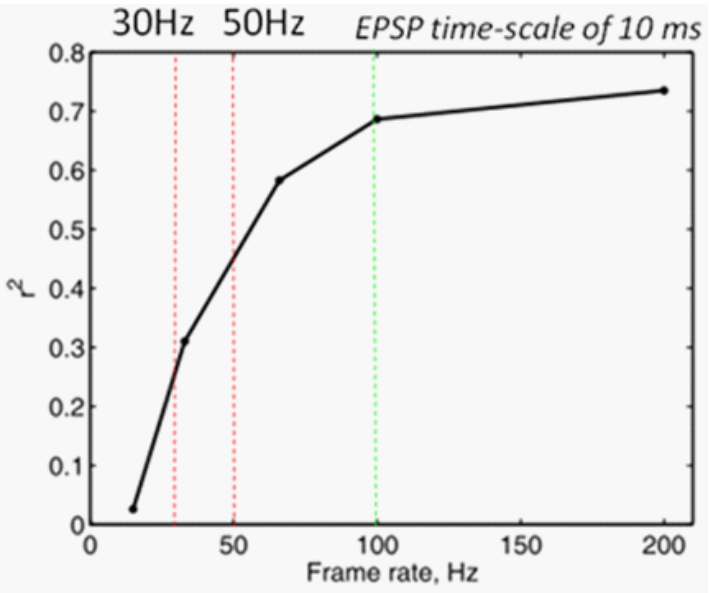

Figure 1: Accuracy of the inferred connectivity matrix as a function of the frame rate of calcium imaging for a simulated population of N=25 realistic cortical neurons, spontaneously firing at an average 5 Hz and observed for T = 10 min with eSNR=10. The reconstructions are quantified using the correlation square measure, r^2, of the actual and the reconstructed connection weights. The imaging frame rate of at least 30 Hz is necessary for reasonable quality of the connectivity reconstructions.

The origin of the figure 30 Hz can be understood as follows. For calcium imaging with the frame size of Δ_F milliseconds, the spikes observed within single frame cannot contribute to the estimation of connectivity matrix because the temporal precedence of such spikes, and thus the causality between them, becomes lost. In other words, although the statistical excess of coincident spikes within a single imaging frame can and will indicate the presence of a connection between neurons, such excess cannot be used to establish whether such connections are from neuron A to neuron B or vice versa, since either will result in exactly the same statistics of the spikes observed within the same imaging frame. The necessary causality information is only obtained for the spikes separated over different calcium imaging frames. Observations of such spikes contain the necessary information to determine the presence of a connection between two neurons as well as its direction. However, the problem with such spikes is that they are separated by times of the order of at least Δ_F, which for durations of Post-Synaptic Potentials **(PSP)** τ_{PSP} much smaller than Δ_F results in the loss of correlations between such spikes. For instance, if we model the decay of the PSPs using an exponential with time scale τ_{PSP}, it becomes clear that in order to detect neural connections with any degree of confidence one needs to have approximately $\exp\left(-\Delta_F/\tau_{PSP}\right) > 0.1$ or Δ_F/τ_{PSP} of at most 3, which leads to the largest acceptable imaging frame of $\Delta_F \approx 30$ milliseconds and the imaging frame rate of 30 Hz, for typical cortical $\tau_{PSP} \approx 10$ milliseconds [92].

To summarize, the low frame rate of calcium imaging can have strong detrimental effects on one's ability to infer connectivity graphs from calcium imaging data. This is irrespective of one's ability to detect individual spikes and is entirely related to the loss of causal relationships between neural spikes observed over neighbor calcium imaging frames, when such frames are much larger than the extent of typical PSPs. The spikes observed within the same calcium imaging frame cannot be used for estimation of neural connectivity as they do not possess the precedence information necessary to establish causality. In order to use population calcium imaging for neural connectivity inference, therefore, it is necessary for the calcium imaging frame rates to be at least 30 Hz and possibly 50 Hz and higher.

The second essential parameter of calcium imaging that strongly affects the possibility of neural connectivity inference is the signal-to-noise ratio or SNR. SNR may be a tricky quantity to define for experimentalists, as there are many types of signal and noise in a typical practical calcium imaging scenario. For instance, one has photon shot-noise, background fluorescence noise, molecular noise in calcium concentrations, noise in optical device, etc. One can use an effective SNR definition to circumvent these complexities, which effectively quantifies the ratio of the spike-related jumps in calcium fluorescence to the typical variation in calcium fluorescence signal;

$$eSNR = \frac{E\left[\left|F(t) - F(t-\Delta)\right| n(t) = 1\right]}{E\left[\left(F(t) - F(t-\Delta)\right)^2 / 2 \middle| n(t) = 0\right]^{1/2}} \tag{7}$$

The qualitative examples of such calcium fluorescence signals for different values of effective SNR are shown in Figure 2. The survey of the neural connectivity inference from simulated calcium imaging data with different values of eSNR shows that eSNR of about 5 and above is required for successful neural connectivity inference, Figure 3. At the same time, eSNR above approximately 9 does not result in further improvements in one's ability to estimate neural connection weights, and eSNR below 3 certainly results in the imaging data that cannot be used for estimation of single-cell neural connectivity. The accuracy of reconstructed connectivity matrices plateaus at a given level as the eSNR grows, which is defined by the frame rate of imaging, in lieu with the above discussion. Thus, for the imaging frame rate of 15 Hz, no amount of SNR suffices to enable one's estimation of neural connectivity, for instance.

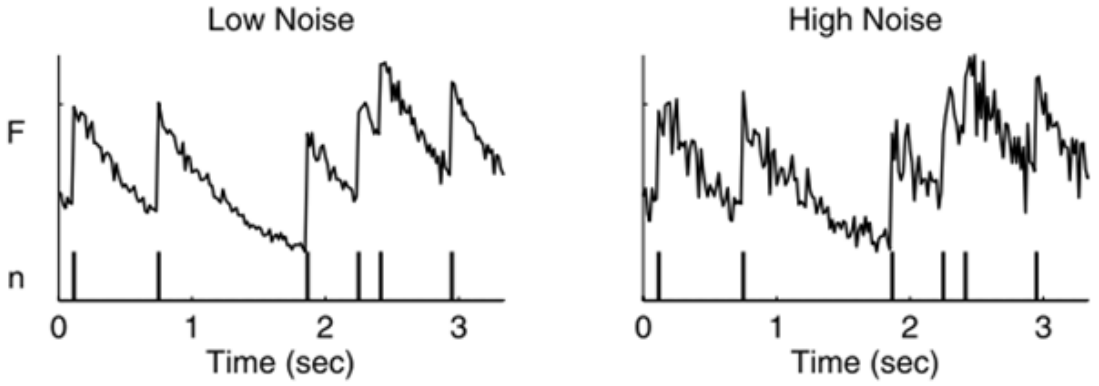

Figure 2: Two examples of simulated calcium fluorescence data for eSNR=9 (left, low noise) and eSNR=3 (right, high noise).

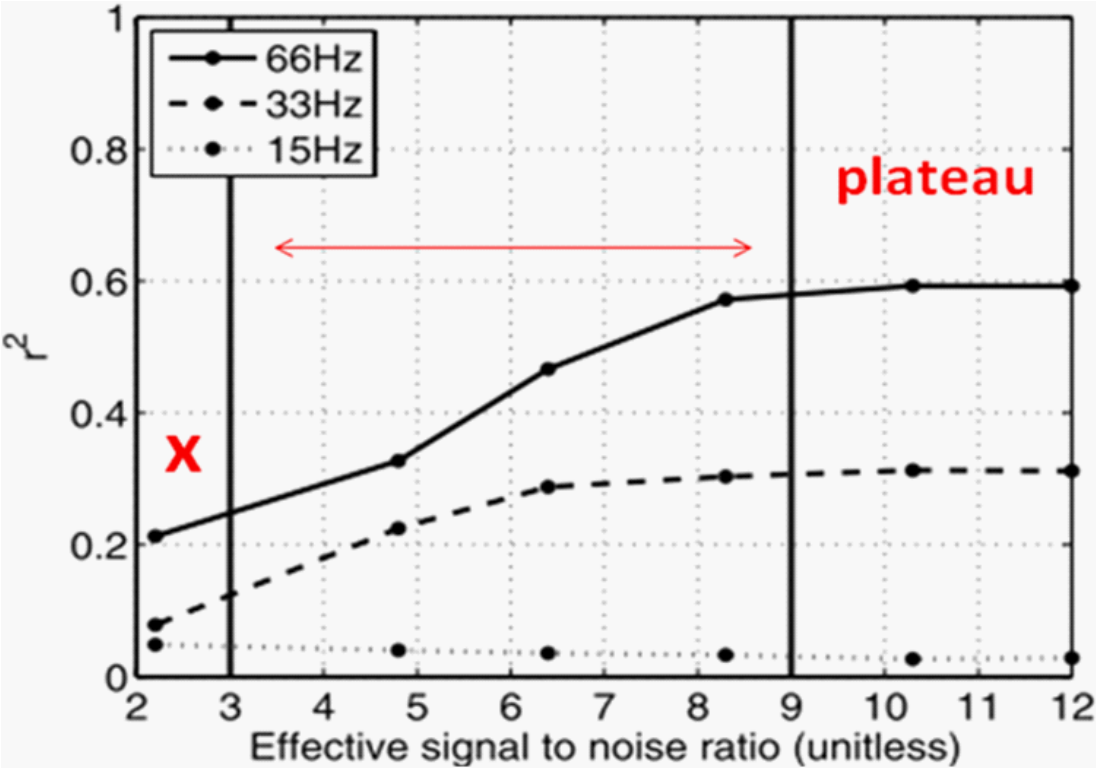

Figure 3: Accuracy of inferred connectivity as a function of the effective calcium imaging signal-to-noise ratio (eSNR, Eq. (7)) for frame rates of 15, 33 and 66 Hz. Neural population simulations are the same as in Figure 1. Vertical black lines correspond to the eSNR values of the two example traces in Figure 2. eSNR greater than about 5 is necessary for neural connectivity reconstructions from population calcium imaging data. eSNR above approximately 9 do not result in further increase in neural connectivity reconstruction accuracy.

With respect to the requirements on the duration of imaging, [54] finds that about 3000 observed spikes per neuron generally are required for the reconstructions of neural connectivity in the simulations of realistic cortical neural networks. For average spontaneous firing rate of 5 Hz in networks simulated in [54], this is stated as the imaging time requirements of approximately 10 minutes, Figure 4. However, the more appropriate measure indeed is the count of spikes per neuron and not such imaging duration. For larger durations of imaging, the accuracy of reconstructed connectivity matrices plateaus at the level prescribed by the frame rate and the eSNR, and the collection of further data does not lead to significant improvements in the connectivity reconstructions.

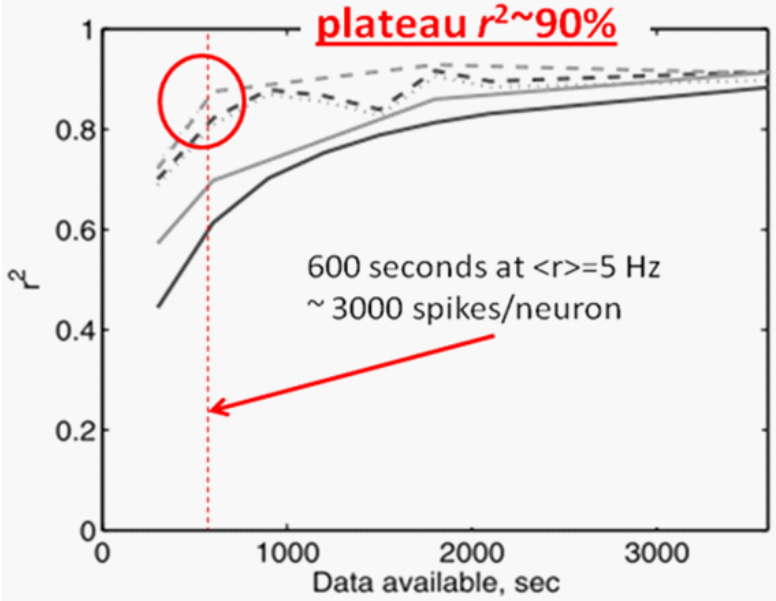

Figure 4: Accuracy of inferred connectivity as a function of the imaging time and neural population size. The minimal imaging time of about T = 10 min or 3000 spikes per neuron is seen as necessary for reconstructions' performance to plateau, with further increase in the imaging time conferring no immediate benefits. Simulation eSNR ≈ 10 and 60 Hz frame rate in every case.

An interesting further observation in [54] is that the required amount of imaging data does not appear to significantly vary with the size of neural populations. Namely, all way to the neural population sizes of about 1000 neurons the required imaging time observed in [54] is 10 minutes or 3000 spikes/neuron. Therefore, [54] observes that longer observations of neural populations are not be required as the size of imaged neural populations gets bigger - the imaging of about 10 minutes of neural population activity at 5 Hz average spontaneous firing rate can be expected to suffice for neural connections' estimation.

Finally, it is observed in [54] that using priors - most importantly sparse prior - is crucial for increasing the speed of convergence of functional connectivity inference. When estimating neural connectivity matrix from population calcium imaging data without using any prior, the performance plateau is achieved at over 3000 seconds of imaging time. However, when additionally enforcing in the inference the constraint that the neural connectivity graph is sparse (as is well known from neurophysiology), the imaging times required for achieving the same plateau drop to about 600 seconds. The effect on neural connectivity inference conferred by sparse priors, therefore, is very dramatic and should be always used. This effect is illustrated in Figure 5 and Figure 6.

The sparseness of the target connectivity matrix can be enforced in Bayesian connectivity inference by imposing a L1 prior on the connection weights,

$$P(W) = \exp\left(-\lambda \sum_{ij} |W_{ij}|\right). \quad (8)$$

It is not necessary to exactly know the level of sparseness in this estimation, recent results based on Compressive Sensing indicate that a rapid sparsification of the connectivity graph and the increase in its similarity with the ground truth is achieved as long as almost any not increasingly small $\lambda>0$ is used [93].

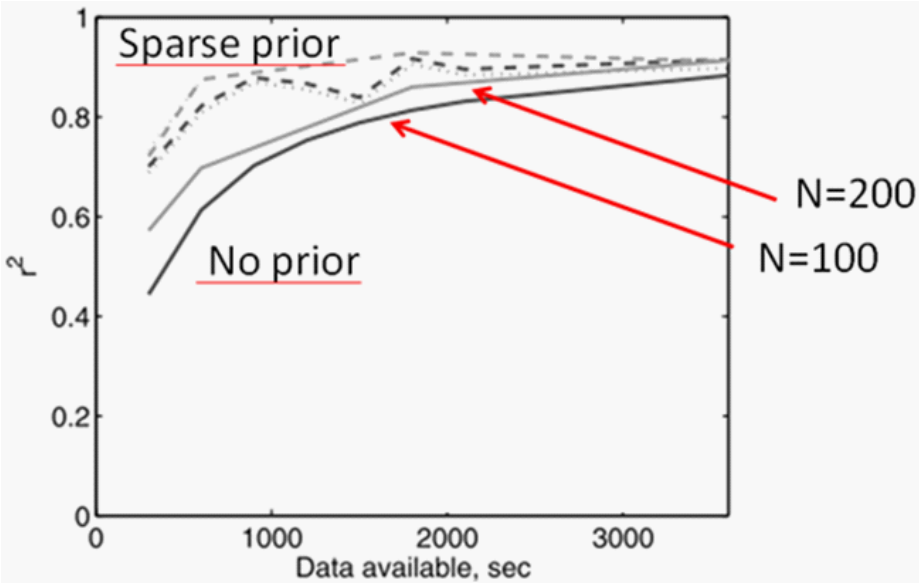

Figure 5: Accuracy of inferred connectivity as a function of the imaging time and neural population size. The minimal imaging time requirement does not show strong dependence on the neural population size. Here, neural populations of size N = 100 and 200 are shown (black and gray, respectively) without significant difference in the r^2 curves. Furthermore, incorporation of a sparse prior can dramatically increase the reconstruction's accuracy (shown by dashed lines). Simulation eSNR ≈ 10 and 60 Hz frame rate in every case.

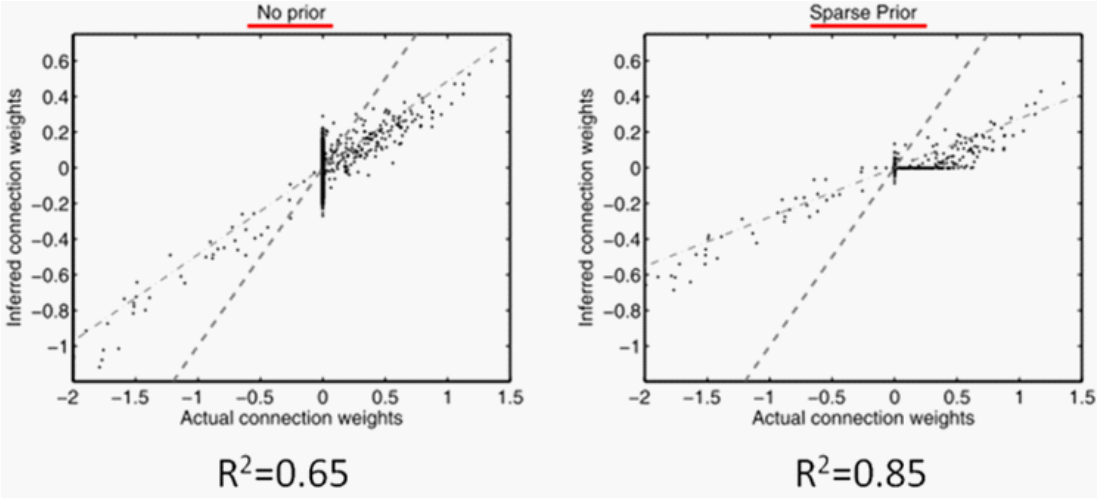

Figure 6: Imposing a sparse prior on the connectivity matrix dramatically improves neural connectivity estimation. Scatter plots show the connection weights W_{ij} reconstructed with (right) and without a sparse prior (left). The simulation is for N = 50 neurons with average spontaneous firing rate 5 Hz, imaged for T = 10 min at frame rate of 60 Hz and eSNR =10.

SPARSE ACTIVITY SAMPPLING SCHEMES FOR LARGE-SCALE NEURAL CONNECTIVITY INFERENCE FROM POPULATION CALCIUM IMAGING

One of the key problems of neural connectivity inference from population calcium imaging is the necessity to simultaneously observe the entire neural population for the reconstruction of the connectivity matrix to become possible. Because functional analysis relies on co-relating the activity of neurons in neural population over extended periods of time, lack of complete observations will result in errors due to missing or unobserved neural inputs interfering with the inference process [57,69,72,75,94,95]. For instance, in the canonical example of "hidden inputs" problem one can mistake the correlations in the activity of several neurons due to their correlated (but not observed) inputs for a direct connection between them. Despite swift progress in large-scale neural activity data acquisition, it is still beyond the reach of current technology to monitor with required temporal resolution the set of all neurons comprising the presynaptic inputs of even a single cortical neuron. Full-brain calcium imaging experiments recently demonstrated in the literature provide the brain-wide coverage at the rates of only 1 Hz to 2 Hz [42,43], and 5 Hz recently in larval Drosophila [42], way below the minimum 30 Hz identified in Section 2.

An approach that can allow neuroscientists to overcome this problem already with today's technology - the shotgun or sparse neural activity imaging - had been recently proposed in [78,79,96,97]. In this approach, large neuronal populations are suggested to be imaged partially or sparsely in random or deterministic sequence, imaging only a small number of neurons at any given time. Such observations can be collected over extended periods of time using limited

existing calcium imaging capabilities. Although each such observation or set of observations is grossly incomplete, [78,79,96,97] show that it is in fact possible to extract the complete correct neural connectivity matrix from such measurements, as long as certain basic requirements are met related to the organization of imaging experiments.

A deeper theoretical look into this problem had been taken in [78], and it was shown that the reconstractability of complete connectivity graphs from sparse neural activity data is related to coverage by the observations of certain uniquely identifying sets of neural population's subpopulations. For several practically important classes of neural activity models, [78] proved that the set of such uniquely identifying observations consists of all pair-wise input-output neural activities $\left(n_i\left(t+\Delta\right), n_j\left(t\right)\right)$ or the neural activity triples of the form $\left(n_i\left(t+\Delta\right), n_j\left(t\right), n_k\left(t\right)\right)$. That is, in order to reconstruct the complete connectivity graph of entire neural populations, it is only necessary to collect a sufficient number of observations of all neural pairs firing in input-output configurations or the neural activity triples consisting of the same-time neural spiking of all neural pairs together with subsequent firing of a third neuron, for all combinations of such triples.

More specifically, [78] inspects parametric models of neural population activity that can be written in the form $P\left(\chi\middle|W\right)$, where W is the connectivity matrix parameter defining the neural connectivity graph, χ is the neural population's raster of historical activity, and $P\left(\chi\middle|W\right)$ is the probability of observing a given realization of χ given W. In sparse neural activity imaging, one tries to infer the connectivity matrix from a collection of incomplete and partial observations of neural population's activity. We can say then that one tries to estimate the neural connectivity graph W in $P\left(\chi\middle|W\right)$ from a set of partial observations of neural activity $X\subset\chi$. The central Theorem 1 proven in [78] shows that:

Theorem 1 from [78]: Let $P\left(\chi\middle|W\right)$ be a statistical model of neural population activity $\chi=\left\{n_i\left(t\right), t=0,\Delta,2\Delta....\ \&\ i=1,....,N\right\}$ and let $S=\left\{S\left(t\right), t=0,\Delta,2\Delta...\right\}\sim P\left(S\right)$ be a model of partial observations of that activity over sub populations of neurons S(t). Let χ and S jointly define a stationary and ergodic stochastic process, and also assume that the model $P\left(\chi\middle|W\right)$ is uniquely identified by a set of partial activity distributions $\boldsymbol{P}\left(\boldsymbol{S}\right)=\left\{P\left(\chi_{S(0:k\Delta)}\left(t:t+k\Delta\right)\middle|W\right), S\left(0:k\Delta\right)\in\boldsymbol{S}\right\}$ for some $\boldsymbol{S}$, in the sense that for any $W\neq W'$ there exist at least one $S\left(0:k\Delta\right)\in\boldsymbol{S}$ such that $P\left(\chi_{S(0:k\Delta)}\left(t:t+k\Delta\right)\middle|W\right)\neq P\left(\chi_{S(0:k\Delta)}\left(t:t+k\Delta\right)\middle|W'\right)$, where $\chi_{S(0:k\Delta)}\left(t:t+k\Delta\right)$ means the restriction of $\chi\left(t:t+k\Delta\right)$ to the sequence of subpopulations $S\left(0:k\Delta\right)$. Then, under weak technical conditions necessary for the convergence of maximum likelihood estimation, for any model of partial observations P*(S)* such that the support $\boldsymbol{S}'=\left\{S\left(0:k\Delta\right): P\left(S\left(0:k\Delta\right)\right)>0\right\}$ completely covers ***S***, the ML estimator

$$\widehat{W}_T\left(\chi,S\right)=\arg\max_{\widehat{W}} L\left(\widehat{W}\middle|\chi,S;T\right), \tag{9}$$

where

$$L\left(\widehat{W}\middle|\chi,S;T\right)=\sum_{t=0}^{T}\log P\left(\chi_{S(t:t+k\Delta)}(t:t+k\Delta),S(t:t+k\Delta)\middle|\widehat{W}\right), \tag{10}$$

converges to the true value of W as T→∞ (that is, is consistent).

Theorem 1 establishes that under very general conditions the sparse observations of neural population activity can be used to uniquely identify the complete connectivity matrix in an entire neural population. Theorem 1 only requires that (i) the rules governing the dynamics of the neural population and the selection of the sparse observed subpopulations are time invariant (stationarity), (ii) the neural dynamics is rich enough to explore the entire state space and not get trapped in its small parts (ergodicity) and (iii) observed neural subpopulations cover a special uniquely identifying set of partial neural activity distributions **P(S)**. Theorem 1 shifts the burden of establishing the reconstructability of neural connectivity matrix in sparse neural activity imaging settings to determining the *uniquely identifying* sets of particular neural activity models. In [78], arguments are presented to expect that the coverage of all pair-wise input-output neural activity distributions $P\left(n_i(t+\Delta),n_j(t)\middle|W\right)$ is sufficient for at least locally unique reconstruction of complete connectivity matrices in a very general class of network models of neural population activity. [78] also provides several rigorous theorems and corollaries that establish slightly weaker but still highly advantageous uniquely identifying sets for several practically important models of neural population activity. Namely, Theorem 3 in [78] states;

Theorem 3 from [78]: Consider a family of general "network type" models of neural population activity characterized by a N×N connectivity matrix W and a transition probability density

$$P\left(\chi(t):\chi(t-\Delta)\right)=\prod_{i=1}^{N}P\left(n_i(t)\middle|W_i\chi(t-\Delta)\right), \tag{12}$$

where W_i is the i^{th} row of the connectivity matrix W and $N=\dim\left(\chi(t)\right)$. Let model (12) define an ergodic stochastic process and let $\log P\left(\chi(t)\middle|\chi(t-\Delta);W\right)$ be L1 integrable under the stationary distribution of that process. Also let $l_{T,N}\left(W\middle|\chi\right)$ be the average log-likelihood function given the realizations of neural activity patterns $\chi=\left\{n_i(t),t=0,\Delta,....,T\ and\ i=1,...,N\right\}$ in model (12),

$$l_{T,N}\left(W\middle|\chi\right)=\frac{1}{NT}\sum_{t=0}^{T}\sum_{i=1}^{N}\log P\left(n_i(t)\middle|W_i\chi(t-\Delta)\right). \tag{13}$$

Then, if the sums $J_i(t)=\sum_{j=1}^{N}W_{ij}n_j(t-\Delta)$ tend to Normal distribution as N→∞ (the Central Limit Theorem), the set of all triple-activity distributions $P\left(n_i(t+\Delta),n_j(t),n_k(t)\right)$ is uniquely identifying in model (12) in the limit N→∞, and also $l_{T,N}\left(W\middle|\chi\right)\to l_\infty(W)\,as\,T,N\to\infty$, where

$$l_\infty(W)=\frac{1}{N}\sum_{i=1}^{N}\int dn_i dJ_i\log P\left(n_i\middle|J_i+W_i\mu_i(n_i)\right)\frac{e^{-J_i^2/\left(2W_i\Sigma(n_i)W_i^T\right)}}{\sqrt{2\pi W_i\Sigma(n_i)W_i^T}} \tag{15}$$

and $\mu(n_i)=E\left[\chi(t)\middle|n_i(t+\Delta)=n_i\right]$ and $\Sigma(n_i)=\mathrm{cov}\left(\chi(t)\middle|n_i(t+\Delta)=n_i\right)$.

Corollary 3 of Theorem 3 in [78] establishes for the exponential GLM of neural activity [93] that the identifying sets are $P\left(n_i(t+\Delta), n_j(t)\middle|W\right)$, all i and j, and also that Eq. (15) is $l_\infty(W) = \mu^T b + Tr\left[W\Sigma_1^T\right] + \Sigma_{i=1}^N e^{b_i + W_i\mu + 2W_i\Sigma W_i^T}$, with $\mu = \mathrm{E}\left[\chi(t)\right], \Sigma_1 = \mathrm{E}\left[\chi(t+\Delta)\chi(t)^T\right]$ and $\Sigma = \mathrm{cov}\left(\chi(t)\right)$.

The above results from [78] rigorously establish that it is only needed to collect the observations of particular uniquely identifying sets of partial neural activity distributions to be able to uniquely reconstruct the full connectivity matrix from sparse observations of a neural population's activity. In a very general class of neural population activity models such indentifying sets are small, requiring only the observations of all pairs of input-output neural activities $P\left(n_i(t+\Delta), n_j(t)\middle|W\right)$ or the triple distributions $P\left(n_i(t+\Delta), n_j(t), n_k(t)\right)$. Collecting such observations is immeasurably simpler than procuring the simultaneous observation of an entire macroscopically large neural ensemble. Such sparse observations, nevertheless, are equailly sufficient for identifying the connectivity graphs in such large neural populations.

Another important aspect of Theorem 1 is that it is not important how the coverage of the identifying sets is provided. It is only important that such coverage is complete. For instance, a plausible full connectivity matrix estimation strategy is to image the input-output activity of neurons one pair of neurons at a time, in any order. Theorem 1 also implies that it is not important how the uniquely identifying sets constrain the complete connectivity matrix W or by means of which statistics W can be calculated. Whenever the uniquely identifying coverage had been provided, using either a non-deterministic or a reasonable deterministic protocol, Theorem 1 establishes that the complete connectivity matrix can be recovered via the MLE given by Eq. (9) and (10).

Theorem 3 and related corollaries in [78] also offer some advantageous ways for calculating the neural connectivity graphs from sparse imaging data, by using Eq. (15) and its derivatives. For instance, if the conditions of Theorem 3 hold, one can solve for the maximum of the expected log-likelihood $l_\infty(W)$ in order to find W. $l_\infty(W)$ depends in a relatively simple way on the statistics $\mu(n_i)$ and $\Sigma(n_i)$. These can be estimated easily from the sparse spike trains data collected in a "shotgun-like" neural activity imaging experiment. This can greatly simplify the connectivity matrix inference and even make it possible to calculate the connectivity matrix in online manner, for example, for use in adaptive experiment designs.

[78] builds on these findings to introduce a new neural activity imaging design, significantly more advantageous experimentally and computationally to the original shotgun proposal made in [97]. While observing the neurons completely randomly, as in [97], does guarantee that all possible subsets of neurons are covered in such an imaging, strictly random observation of neurons is highly challenging to implement experimentally. [78] capitalizes on the findings that only the coverage of the identifying sets of neural subpopulations is important and not the manner in which such coverage is provided, to propose an alternative deterministic organization

of sparse imaging named "block-wise round-robin sampling strategy". In this protocol, neural population is imaged in two or more spatially contiguous blocks by means of two or more scanning microscopes. At every time, a fixed configuration of such blocks is observed so that a certain set of examples of neural input-output activity tuples is provided. Over the course of the experiment, the blocks are moved through the neural population to produce all required combinations, such as discussed above, Figure 7.

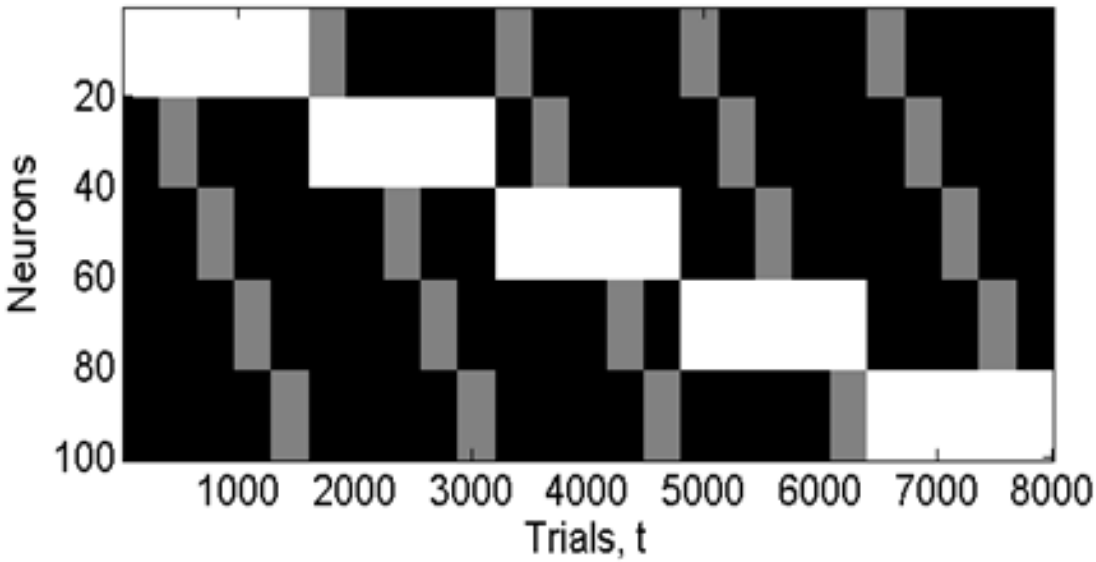

Figure 7: Block-wise round-robin neuronal activity imaging strategy. In this strategy, neuronal population is imaged as a sequence of spatially-contiguous blocks of neurons. During one section of the experiment, all neurons in each block are observed simultaneously for a given duration of time T_b .The blocks are gradually moved throughout the experiment to achieve all possible combinations of the blocks. This figure illustrates the block-wise round-robin sampling strategy applied to a hypothetical population of 100 neurons with 20 neurons observed in one input and one output block. White color indicates the neurons in the output blocks and gray color indicates the neurons in the input blocks. In each observation, the activity of all marked neurons should be observed simultaneously. Over the entire experiment, all pairs of neurons in input-output configuration are observed, providing the foundation for uniquely reconstructing the complete neural connectivity matrix.

Block-wise round-robin imaging organization guarantees the coverage of all neural activity tuples necessary for the reconstructions of complete connectivity matrix, as discussed above. In this sense, it is sufficient for the reconstruction of complete neural populations' connectivity graphs. It has further advantage of being straightforward to implement using existing calcium imaging techniques as well as having a simpler numerical connectivity estimation problem.

Conceptual and technical simplicity of the block-wise round-robin sparse neuronal activity imaging gives hope that it can be realized for imaging of real biological neural systems in near future.

The key tradeoff made in the sparse neural activity imaging is that of increased noise in the connectivity reconstructions. This issue is also studied in detail in [78], and the following approximate formula is obtained for estimating the posterior variance of the neural connection weights estimator in sparse imaging settings,

$$\mathrm{var}\left(\widehat{W}\right) \propto sN_h A_w^2 \Big/ T_b \,. \tag{17}$$

Here, s is the sparseness of neural connectivity, N_h is the typical size of hidden or unobserved neural populations, $A_w^2 = < W_{ij}^2 > w_{ij \neq 0}$ is the rms strength of nonzero neural connection weights, and $T_b = p^2 T$ is the observation time for a single input-output neural pair, whereas p is the fraction of neurons contained in one observation. This formula shows that the noise in sparse neural connectivity reconstructions, and the imaging time needed to overcome it, will grow proportionally to the number of unobserved neurons, the square of typical connection strength, and the inverse square of the fraction of neurons covered in a typical observation. For small fractions p, large sizes of hidden populations N_h or strong connectivity these will result in significantly longer observation times necessary for sparse neural activity imaging, as compared to complete observations of neural populations' activity. These scalings are inopportune for experimental setups where the number of unobserved neurons will remain large or the fraction of observed neurons will need to remain small. However, it should be possible to overcome these obstacles, especially, in *in-vivo* calcium imaging experiments, such as recently demonstrated in [36,40,42-44,46,48-51].

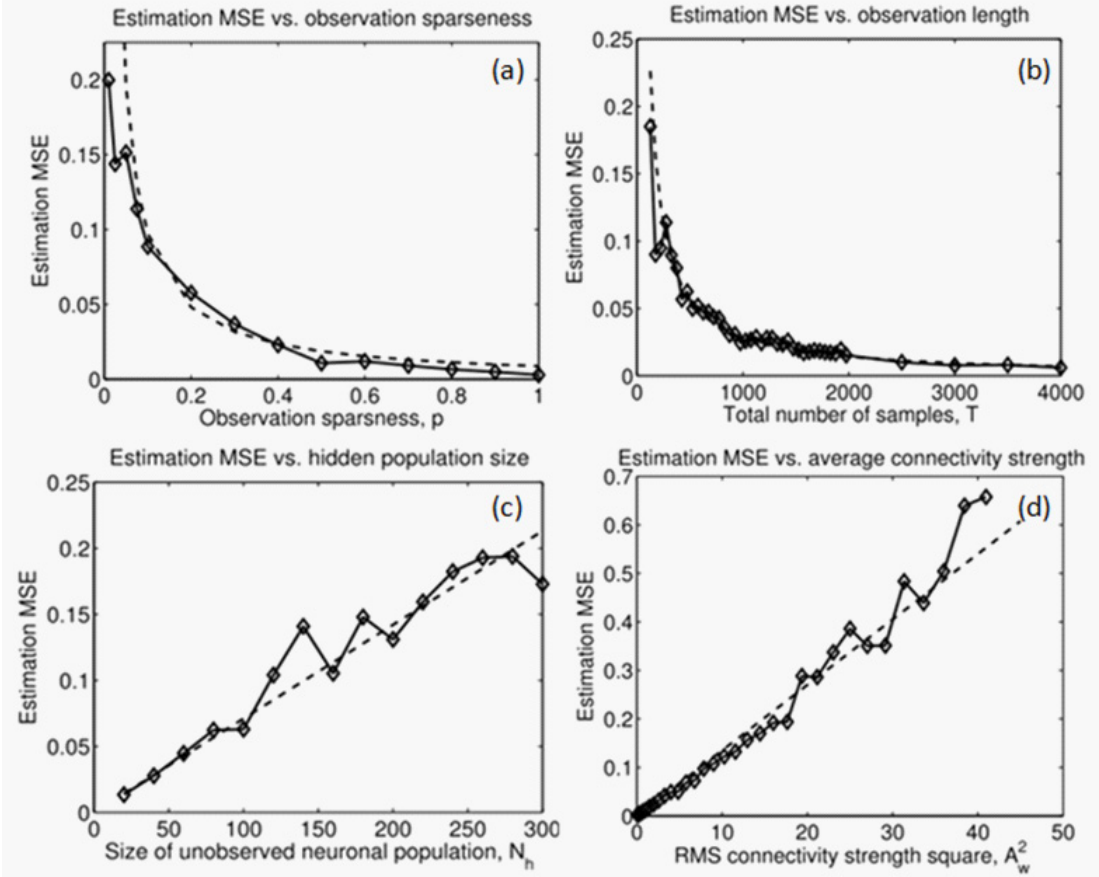

Figure 8: The properties of sparse connectivity imaging in relation to the missing data. From top to bottom, the posterior error of the sparse connectivity estimates is shown in relation to the observations' sparseness (a), the total number of observation samples (b), the size of the hidden populations (c), and the rms-average connectivity strength (d). The results of numerical simulations are shown with solid line and dashed lines show the theoretical predictions given formula (17).

EFFECTIVE CONNECTIVITY FRAMEWORK FOR NEURAL CONNECTIVITY MODELING AND RECONSTRUCTIONS

It is important to point out that the above computational and theoretical work departs from and is grounded in the framework of statistical modeling of neural population activity, such that can be succintly encompassed by the formula $P(x|W)$. The estimates of neural connectivity thus discussed, either for complete-observations case discussed in Section 2 or sparse imaging case discussed in Section 3, are therefore for the parameter W of such neural activity models. Thus, it may be proper to ask: what is the significance and the relation of such model parameter W to the real neural circuit connectivity we are seeking in neuroscience?

It needs to be realized that the concept of neural connectivity needed for the answer to this question unfortunately lacks clarity. Although a significant effort has been directed in neuroscience at empirically extracting the neural connectivity in real biological systems, the definition and the nature of such connectivity remained to large extent uncertain and varying from author to author.

The oldest view on neural connectivity is characterized by identifying neural connectivity with the physical connections graph of a neural circuit. This point of view dates back to the works of Cajal and became the basis of the classical work in *C. elegans* [98], where the connectivity graph of the entire nervous system of *C. elegans* had been painstakingly reconstructed from serial electron microscopy and recorded in the form of the graph of physical synaptic and gap-junction connections in that circuit. An explosion of work pursuing the extraction of such physical connectivity graphs either using electron microscopy, light microscopy, or more sophisticated strategies such as viral tracers or diffusion tracer imaging had occurred in recent years. We can collectively refer to such approach to the study of neural connectivity as structural or synaptic.

An alternative view on the same issue had been provided by functional imaging community, dating back to the electrophysiological studies of past century and recently transforming into an explosion of works using calcium and voltage imaging, fMRI, and EEG neural activity imaging techniques. In this view, the neural connectivity is identified with the correlates of neural activity measured over different parts of the brain. A very impressive body of work in this direction has emerged based on the fMRI data. We can refer to such approach to the study of neural connectivity as functional.

Despite tremendous advances along both of these directions, some key problems are well known to exist within both of these approaches. In the case of structural connectivity, it had become understood that structural connectivity graphs without information describing the dynamics of the connections as well as that of connected neurons cannot lead to the understanding of neural circuits. The studies in *C. elegans* over the past decade done by Cori Bargmann demonstrated that highly nontrivial behaviors can result under the same, and for that matter well known, connectivity graph from nontrivial properties of the neurons themselves, and that even knowing the complete structural connectivity graph such as in *C. elegans*, while invaluable in many respects, cannot sufficiently constrain the variety of the behaviors possible on such a graph without knowledge of the dynamics. In functional connectivity studies, it became understood that the nature and the relation of neural activity correlations to the "real" or physical structure of neural circuits, or even to the causation over such circuits or the ability to make predictions, is uncertain. It became unclear what implications functional connectivity graphs should have for the understanding of the brain's function or how they should be used in predictive or explorative contexts.

In this work, I would like to put forth alternative viewpoint that the interpretation of neural connectivity as the above parameter of a defined, statistical, descriptive, and causal model of neural population activity offers a superior analytical framework for deciphering the properties and the workings of neural circuits. Adopting such framework for the design and analysis of real

neural activity imaging experiments can provide significant advantages both from the point of view of mechanistic interpretation of neural connectivity and activity as well as from the point of view of using these for exploratory and predictive purposes. This aproach can be called effective connectivity.

Effective models of neural connectivity can be defined as the network-type statistical models of neural population activity that are fitted to describe the behavior of real experimentally observed neural populations. An example of such a model can be given by Eq. (6) in Section 2, or more generally by $P(\chi|W)$ such as was used to formalize the sparse neural connectivity inference problem in Section 3. The matrix of the connection weights in such models can be called the effective connectivity matrix of the corresponding observed neural population.

Effective models of neural connectivity most typically are the network models of neural activity. Such models may differ in the levels of detail and realisticity. For instance, one may design extremely detailed such a model consisting of a population of coupled Hodgkin-Huxley neurons with conductive synapses and electric gap-junctions, supplemented with the model of internal neural evolution responsible for the attenuation of the strengths of the synapses and other effects. The concept of effective connectivity is such that, if the model of neural population's dynamics is as accurate with respect to the physiological reality of individual neurons as the model above, then the effective connectivity in such a model is precisely the structural or the synaptic connectivity such as exists in the corresponding circuit.

Of course, in most cases one has to use more approximate models of neuronal dynamics for the reason of tractability. Whereas a detailed Hodgkin-Huxley-type model of neural dynamics may be very attractive for fundamental reasons, such a model can be computationally expensive to calculate and the fitting procedure may not converge due to numerous local optima or extreme singularities. These may make fitting such realistic effective models to real data collected in large quantities practically impossible. One needs to strike a balance between realism and tractability.

A class of simpler yet very successful effective models of neural activity, very popular in computational and theoretical neuroscience, is the LIF models. Another highly attractive class is the generalized linear models, shown to be equivalent to LIF under certain conditions, and used to model the properties and the behavior of real Ganglion cells in retina [53,58,99-101]. Although such models had been found to not necessarily reproduce the anatomical structure of the connectivity of the populations of Ganglion cells in retina, one needs to draw attention here to the success of such models in describing the behavior of the measured neural populations. It is that ability to successfully capture and describe the activity of real neural circuits that I suggest is the key aspect of the concept of effective connectivity that can prove highly advantageous in neuroscience.

More specifically, once we focus on that aspect of effective connectivity, we can realize that the effective connectivity models of neural population activity offer extremely important qualities of being causal, generative, and predictive with respect to the description of neural dynamics in specific and real neural populations, even if such models may not - and most likely will not - be directly equal to the anatomical connectivity in such neural populations. Given that property, such models allow predicting the behavior and responses of real neural systems to novel stimuli and conditions, as well as offer insights into the causal pathways that the information takes in such real neural systems. These extremely important qualities allow the effective connectivity models to be used for;

i. Generating examples of neural activity for real neural populations.

ii. Quantitatively comparing and verifying such examples versus experiments.

iii. Predicting how the patterns of neural activity develop throughout neuronal circuits, possibly causally, depending on the causality supplied by the model.

iv. Predicting the responses of real neural population to a change in external or internal conditions, and verifying such predictions experimentally.

The points (i) through (iv) are the key ingredients of the loop "*Observe-Explain-Predict*" of the basic scientific method and, thus, can prove very valuable for forming the analytical foundation for quantitative and principled understanding of the workings of real neural systems in the brain.

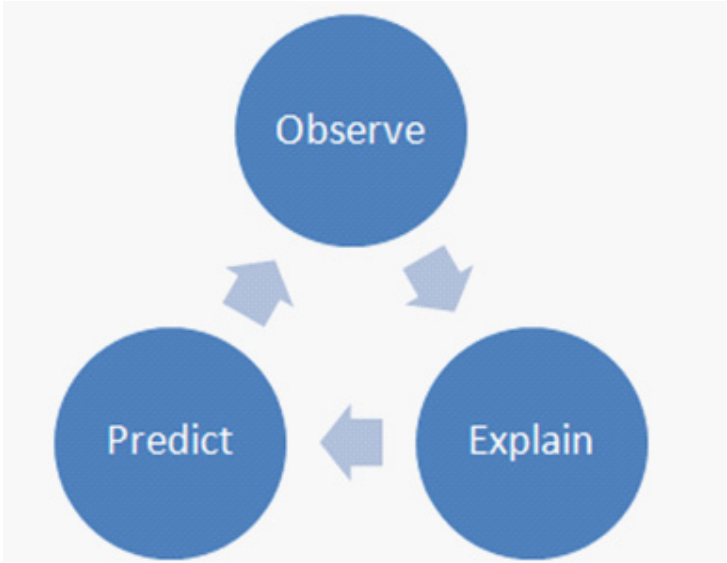

Figure 9: The theoretical estimation formalism presented here together with existing experimental population calcium imaging capacities, within the framework of effective connectivity models, allows principled and quantitative implementation of the Observe-Explain-Predict scientific method's loop by: collecting observations of complete or brain-wide neural population activity using the formalism of sparse neural activity imaging presented in Section 3, deriving the effective models of neural connectivity using the formalism of Section 2, making predictions about neural populations' responses to external or internal perturbations within the framework of effective connectivity models, and quantitatively verifying such predictions experimentally as well as modifying such models with the new measurements.

CONCLUSION

This chapter provided an overview and an introduction to some key developments related to the analysis of calcium imaging data in computational neuroscience. Recent years had seen important advances both in the problem of deconvolution of neural spike trains from calcium imaging data as well as the solutions for the inference of connectivity from population calcium imaging on very large scales had been introduced. A particularly important advancement can be seen in the recent development of the concept of sparse neural population activity imaging and connectivity inference from such data, as well as the detailed elaboration of the key properties of such inference. These developments make it now possible to realize the reconstructions of complete neural connectivity in macroscopically large neural circuits from calcium imaging data using available technologies. Together with the framework of effective neural connectivity, these can serve as the foundation for rapid and significant advancements in quantitative understanding of the working of neural circuits in the brain.

References

1. y Cajal S. La Textura del Sistema Nerviosa del Hombre y los Vertebrados. Moya. 1904.
2. y Cajal S. Recuerdos de mi vida: Historia de mi labor cientifica. Alianza Editorial. 1923.
3. Markram H, Muller E, Ramaswamy S, Reimann MW, Abdellah M, et al. Reconstruction and simulation of neocortical microcircuitry. Cell. 2015; 163: 456-492.
4. Shepherd GMG, Pologruto TA, Svoboda K. Circuit analysis of experience-dependent plasticity in the developing rat barrel cortex. Neuron. 2003; 38: 277-289.
5. Bureau I, Shepherd GMGM, Svoboda K. Precise development of functional and anatomical columns in the neocortex. Neuron. 2004; 42: 789-801.
6. Hagmann P, Kurant M, Gigandet X, Thiran P, Wedeen V, et al. Mapping human whole-brain structural networks with diffusion MRI. PLoS One. 2007; 2: e597.
7. Sato TR, Gray NW, Mainen ZF, Svoboda K. The functional microarchitecture of the mouse barrel cortex. PLoS Biol. 2007; 5: e189.
8. Smith SJ. Circuit reconstruction tools today. Curr Opin Neurobiol. 2007; 17: 601-608.
9. Hagmann P, Cammoun L, Gigandet X, Meuli R, Honey CJ, et al. Mapping the structural core of human cerebral cortex. PLoS Biol. 6: e159.
10. Luo L, Callaway EM, Svoboda K. Genetic dissection of neural circuits. Neuron. 2008; 57: 634-660.
11. Bohland JW, Wu C, Barbas H, Bokil H, Bota M, et al. A proposal for a coordinated effort for the determination of brainwide neuroanatomical connectivity in model organisms at a mesoscopic scale. PLoS Comput Biol. 2009; 5: e1000334.
12. Helmstaedter M, Briggman KL, Denk W. 3D structural imaging of the brain with photons and electrons. Curr Opin Neurobiol. 2008; 18: 633-641.
13. BRAIN: The Brain Research through Advancing Innovative Neurotechnologies Initiative.
14. Human Brain Project Initiative.
15. Plaza SM, Scheffer LK, Chklovskii DB. Toward large-scale connectome reconstructions. Curr Opin Neurobiol. 2014; 25: 201-210.
16. Helmstaedter M. Cellular-resolution connectomics: challenges of dense neural circuit reconstruction. Nat Methods. 2013; 10: 501-507.
17. Sotiropoulos SN, Jbabdi S, Xu J, Andersson JL, Moeller S, et al. Advances in diffusion MRI acquisition and processing in the Human Connectome Project. Neuroimage. 2013; 80: 125-143.
18. Sunkin SM, Ng L, Lau C, Dolbeare T, Gilbert TL, et al. Allen Brain Atlas: an integrated spatio-temporal portal for exploring the central nervous system. Nucleic Acids Res. 2013; 41: D996-D1008.
19. Hatsopoulos NG, Ojakangas CL, Paninski L, Donoghue JP. Information about movement direction obtained from synchronous activity of motor cortical neurons. Proc Natl Acad Sci U S A. 1998; 95: 15706-15711.
20. Harris KD, Csicsvari J, Hirase H, Dragoi G, Buzsaki G. Organization of cell assemblies in the hippocampus. Nature. 2003; 424: 552-556.
21. Stein RB, Weber DJ, Aoyagi Y, Prochazka A, Wagenaar JBM, et al. Coding of position by simultaneously recorded sensory neurones in the cat dorsal root ganglion. J Physiol. 2004; 560: 883-896.
22. Paninski L, Pillow J, Simoncelli E. Comparing integrate-and-fire models estimated using intracellular and extracellular data. Neurocomputing. 2005; 65: 379-385.
23. Truccolo W, Eden UT, Fellows MR, Donoghue JP, Brown EN. A point process framework for relating neural spiking activity to spiking history, neural ensemble, and extrinsic covariate effects. J Neurophysiol. 2005; 93: 1074-1089.
24. Santhanam G, Ryu SI, Yu BM, Afshar A, Shenoy KV. A high-performance brain-computer interface. Nature. 2006; 442: 195-198.
25. Luczak A, Bartho P, Marguet S, Buzsaki G, Harris KD. Sequential structure of neocortical spontaneous activity *in vivo*. Proc Natl Acad Sci U S A. 2007; 104: 347-352.
26. Pillow JW, Shlens J, Paninski L, Sher A, Litke AM, et al. Spatio-temporal correlations and visual signalling in a complete neuronal population. Nature. 2008; 454: 995-999.
27. Antic SD, Empson RM, Knöpfel T. Voltage imaging to understand connections and functions of neuronal circuits. J Neurophysiol. 2016; 116: 135-152.

28. Baker BJ, Kosmidis EK, Vucinic D, Falk CX, Cohen LB, et al. Imaging brain activity with voltage- and calcium-sensitive dyes. Cell Mol Neurobiol. 2005; 25: 245-282.

29. Peterka DS, Takahashi H, Yuste R. Imaging voltage in neurons. Neuron. 2011; 69: 9-21.

30. Tsien RY. Fluorescent Probes of Cell Signaling. Annu Rev Neurosci. 1989; 12: 227-253.

31. Yuste R, Konnerth A, Masters BR. Imaging in Neuroscience and Development, A Laboratory Manual. J Biomed Opt. 2006; 11: 019902.

32. Cossart R, Aronov D, Yuste R. Attractor dynamics of network UP states in the neocortex. Nature. 2003; 423: 283-288.

33. Ohki K, Chung S, Chung YH, Kara P, Reid RC. Functional imaging with cellular resolution reveals precise micro-architecture in visual cortex. Neuron. 2005; 433: 597-603.

34. Ikegaya Y, Le Bon-Jego M, Yuste R. Large-scale imaging of cortical network activity with calcium indicators. Neurosci Res. 2005; 52: 132-138.

35. Gobel W, Helmchen F. *In vivo* calcium imaging of neural network function. Physiology (Bethesda). 2007; 22: 358-365.

36. Prevedel R, Yoon YG, Hoggmann M, Pak N, Wetzstein G, et al. Simultaneous whole-animal 3D-imaging of neuronal activity using light-field microscopy. Nat Methods. 2014; 11: 727-730.

37. Grewe B, Langer D, Kasper H, Kampa BM, Helmchen F. High-speed *in vivo* calcium imaging reveals neuronal network activity with near-millisecond precision. Nat Methods. 2010; 7: 399-405.

38. Dombeck DA, Khabbaz AN, Collman F, Adelman TL, Tank DW. Imaging large-scale neural activity with cellular resolution in awake, mobile mice. Neuron. 2007; 56: 43-57.

39. Zheng M, Cao P, Yang J, Xu XZ, Feng Z. Calcium imaging of multiple neurons in freely behaving C. elegans. J Neurosci Methods. 2012; 206: 78-82.

40. Schrödel T, Prevedel R, Aumayr K, Zimmer M, Vaziri A. Brain-wide 3D imaging of neuronal activity in Caenorhabditis elegans with sculpted light. Nat Methods. 2013; 10: 1013-1020.

41. Greenberg DS, Houweling AR, Kerr JN. Population imaging of ongoing neuronal activity in the visual cortex of awake rats. Nat Neurosci. 2008; 11: 749-751.

42. Lemon WC, Pulver SR, Mcdole K, Branson K, Freeman J, et al. Whole-central nervous system functional imaging in larval Drosophila. Nat Commun. 2015; 6: 7924.

43. Ahrens MB, Orger MB, Robson DN, Li JM, Keller PJ. Whole-brain functional imaging at cellular resolution using light-sheet microscopy. Nat Methods. 2013; 10: 413-420.

44. Ahrens MB, Engert F. Large-scale imaging in small brains. Curr Opin Neurobiol. 2015; 32: 78-86.

45. Peron S, Chen TW, Svoboda K. Comprehensive imaging of cortical networks. Curr Opin Neurobiol. 2015; 32: 115-123.

46. Vladimirov N, Mu Y, Kawashima T, Bennett DV, Yang CT, et al. Light-sheet functional imaging in fictively behaving zebrafish. Nat Methods. 2014; 11: 883-884.

47. Yang W, Miller JE, Carrillo-Reid L, Pnevmatikakis E, Yuste R, et al. Simultaneous Multi-plane Imaging of Neural Circuits. Neuron. 2016; 89: 269-284.

48. Chhetri RK, Amat F, Wan Y, Höckendorf B, Lemon WC, et al. Whole-animal functional and developmental imaging with isotropic spatial resolution. Nat Methods. 2015; 12: 1171-1178.

49. Hildebrand DGC. Whole-brain functional and structural examination in larval zebrafish. Harvard University. 2015.

50. Ahrens MB, Li JM, Orger MB, Robson DN, Schier AF, Engert F, Portugues R. Brain-wide neuronal dynamics during motor adaptation in zebrafish. Nature. 2012; 485: 471-477.

51. Keller PJ, Ahrens MB. Visualizing Whole-Brain Activity and Development at the Single-Cell Level Using Light-Sheet Microscopy. Neuron. 2015; 85: 462-483.

52. Yao Z, Macara AM, Lelito KR, Minosyan TY, Shafer OT. Analysis of functional neuronal connectivity in the Drosophila brain. J Neurophysiol. 2012; 108: 684-696.

53. Vidne M, Ahmadian Y, Shlens J, Pillow J, Kulkarni J, et al. Modeling the impact of common noise inputs on the network activity of retinal ganglion cells. J Comput Neurosci. 2012; 33: 97-121.

54. Mishchenko Y, Vogelstein JT, Paninski L. A Bayesian approach for inferring neuronal connectivity from calcium fluorescent imaging data. Ann Appl Stat. 2011; 5: 1229-1261.

55. Gerhard F, Kispersky T, Gutierrez GJ, Marder E, Kramer M, et al. Successful reconstruction of a physiological circuit with known connectivity from spiking activity alone. PLoS Comput Biol. 2013; 9: e1003138.

56. Timme M, Casadiego J. Revealing networks from dynamics: an introduction. J Phys A Math Theor. 2014; 47: 343001.

57. Vidne M, Kulkarni J, Ahmadian Y, Pillow J, Shlens J, et al. Inferring functional connectivity in an ensemble of retinal ganglion cells sharing a common input. COSYNE. 2009.

58. Field GD, Gauthier JL, Sher A, Greschner M, Machado TA, et al. Functional connectivity in the retina at the resolution of photoreceptors. Nature. 2010; 467: 673-677.

59. Stosiek C, Garaschuk O, Holthoff K, Konnerth A. *In vivo* two-photon calcium imaging of neuronal networks. Proc Natl Acad Sci U S A. 2003; 100: 7319-7324.

60. Wallace DJ, zum Alten Borgloh SM, Astori S, Yang Y, Bausen M, et al. Single-spike detection *in vitro* and *in vivo* with a genetic Ca2+ sensor. Nat Methods. 2008; 5: 797-804.

61. Djurisic M, Antic S, Chen WR, Zecevic D. Voltage imaging from dendrites of mitral cells: EPSP attenuation and spike trigger zones. J Neurosci. 2004; 24: 6703-6714.

62. Iyer V, Hoogland TM, Saggau P. Fast functional imaging of single neurons using random-access multiphoton (RAMP) microscopy. J Neurophysiol. 2006; 95: 535-545.

63. Salome R, Kremer Y, Dieudonne S, Leger JF, Krichevsky O, et al. Ultrafast random-access scanning in two-photon microscopy using acousto-optic deflectors. J Neurosci Methods. 2006; 154: 161-174.

64. Reddy GD, Kelleher K, Fink R, Saggau P. Three-dimensional random access multiphoton microscopy for functional imaging of neuronal activity. Nat Neurosci. 2008; 11: 713-720.

65. Cotton RJ, Froudarakis E, Storer P, Saggau P, Tolias AS. Three-dimensional mapping of microcircuit correlation structure. Front Neural Circuits. 2013; 7: 151.

66. Theis L, Berens P, Froudarakis E, Reimer J, Roman-Roson M, et al. Supervised learning sets benchmark for robust spike detection from calcium imaging signals. bioRxiv. 2015; 010777.

67. Brillinger D. Maximum likelihood analysis of spike trains of interacting nerve cells. Biol Cybernetics. 1988; 59: 189-200.

68. Nykamp DQ. Reconstructing stimulus-driven neural networks from spike times. NIPS. 2003; 15: 309-316.

69. Nykamp DQ. Revealing Pairwise Coupling in Linear-Nonlinear Networks. SIAM J Appl Math. 2005; 65: 2005-2032.

70. Okatan M, Wilson MA, Brown EN. Analyzing functional connectivity using a network likelihood model of ensemble neural spiking activity. Neural Comput. 17: 1927-1961.

71. Srinivasan L, Eden UT, Willsky AS, Brown EN. A state-space analysis for reconstruction of goal-directed movements using neural signals. Neural Comput. 2006; 18: 2465-2494.

72. Nykamp DQ. A mathematical framework for inferring connectivity in probabilistic neuronal networks. Math Biosci. 2007; 205: 204-251.

73. Rigat F, de Gunst M, van Pelt J. Bayesian modelling and analysis of spatio-temporal neuronal networks. Bayesian Anal. 2006; 1: 733-764.

74. Yu B, Afshar A, Santhanam G, Ryu S, Shenoy K, et al. Extracting Dynamical Structure Embedded in Neural Activity. NIPS. 2006.

75. Pillow J, Latham P. Neural characterization in partially observed populations of spiking neurons. In, NIPS. 2007; 1-8.

76. Stevenson IH, Rebesco JM, Hatsopoulos NG, Haga Z, Miller LE, et al. Inferring network structure from spikes. Stat Anal Neural Data Meet. 2008.

77. Stevenson IH, Rebesco JM, Hatsopoulos NG, Haga Z, Miller LE, et al. Bayesian inference of functional connectivity and network structure from spikes. IEEE Trans Neural Syst Rehabil Eng. 2009; 17: 203-213.

78. Mishchenko Y. Consistent estimation of complete neuronal connectivity in large neuronal populations using sparse 'shotgun' neuronal activity sampling. J Comput Neurosci. 2016; 41: 157-184.

79. Soudry D, Keshri S, Stinson P, Oh M, Iyengar G, et al. Efficient 'Shotgun' Inference of Neural Connectivity from Highly Sub-sampled Activity Data. PLOS Comput Biol. 2015; 11: e1004464.

80. Onativia J, Schultz SR, Dragotti PL. A finite rate of innovation algorithm for fast and accurate spike detection from two-photon calcium imaging. J Neural Eng. 2013; 10: 046017.

81. Pnevmatikakis EA, Merel J, Pakman A, Paninski L. Bayesian spike inference from calcium imaging data. In: Asilomar Conference on Signals, Systems and Computers. 2013; 349-353.

82. Vogelstein JT, Packer AM, Machado TA, Sippy T, Babadi B, et al. Fast nonnegative deconvolution for spike train inference from population calcium imaging. J Neurophysiol. 2010; 104: 3691-3704.

83. Mukamei EA, Nimmerjahn A, Schnitzer MJ. Automated analysis of cellular signals from large-scale calcium imaging data. Neuron. 2009; 63: 747-760.

84. Park IJ, Bobkov YV, Ache BW, Principe JC. Quantifying bursting neuron activity from calcium signals using blind deconvolution. J Neurosci Methods. 2013; 218: 196-205.

85. Pnevmatikakis E, Gao Y, Soudry D, Pfau D, Lacefield C, et al. A structured matrix factorization framework for large scale calcium imaging data analysis. arXiv. 2014; 14092903.

86. Sasaki T, Takahashi N, Matsuki N, Ikegaya Y. Fast and accurate detection of action potentials from somatic calcium fluctuations. J Neurophysiol. 2008; 100: 1668-1676.

87. Yaksi E, Friedrich RW. Reconstruction of firing rate changes across neuronal populations by temporally deconvolved Ca2+ imaging. Nat Methods. 2006; 3: 377-383.

88. Vogelstein JT, Watson BO, Packer AM, Jedynak B, Yuste R, et al. Spike inference from calcium imaging using sequential Monte Carlo methods. Biophys J. 2009; 97: 636-655.

89. Yu BM, Shenoy K V, Sahani M. Expectation propagation for inference in non-linear dynamical models with Poisson observations. In: Proceedings of the Nonlinear Statistical Signal Processing Workshop. 2006; 83-86.

90. Paninski L. Maximum likelihood estimation of cascade point-process neural encoding models. Network. 2004; 15: 243-262.

91. Lütcke H, Gerhard F, Zenke F, Gerstner W, Helmchen F. Inference of neuronal network spike dynamics and topology from calcium imaging data. Front Neural Circuits. 2013; 7: 201.

92. Sayer RJ, Friedlander MJ, Redman SJ. The time course and amplitude of EPSPs evoked at synapses between pairs of CA3/CA1 neurons in the hippocampal slice. J Neurosci. 10: 826-836.

93. Mishchenko Y, Paninski L. A Bayesian compressed-sensing approach for reconstructing neural connectivity from subsampled anatomical data. J Comput Neurosci. 2012; 33: 371-388.

94. Vakorin VA, Krakovska OA, McIntosh AR. Confounding effects of indirect connections on causality estimation. J Neurosci Methods. 2009; 184: 152-160.

95. Tyrcha J, Hertz J. Network inference with hidden units. Math Biosci Eng. 2014; 11: 149-165.

96. Turaga S, Buesing L, Packer AM, Dalgleish H, Pettit N, et al. Inferring neural population dynamics from multiple partial recordings of the same neural circuit. In: Neural Information Processing Systems. 2013; 1-9.

97. Keshri S, Pnevmatikakis E, Pakman A, Shababo B, Paninski L. A shotgun sampling solution for the common input problem in neural connectivity inference. arXiv. 2013; 1-9.

98. White J, Southgate E, Thomson JN, Brenner S. The structure of the nervous system of the nematode caenorhabditis elegans. Philos Trans R Soc Lond B Biol Sci. 1986; 314: 1-340.

99. Shlens J, Rieke F, Chichilnisky E. Synchronized firing in the retina. Curr Opin Neurobiol. 2008; 18: 396-402.

100. Shlens J, Field GD, Gauthier JL, Greschner M, Sher A, et al. The Structure of Large-Scale Synchronized Firing in Primate Retina. J Neurosci. 2009; 29: 5022-5031.

101. Ramirez AD, Paninski L. Fast inference in generalized linear models via expected log-likelihoods. J Comput Neurosci. 2014; 36: 215-234.